

Amplitude equations and pattern selection in Faraday waves

Peilong Chen¹ and Jorge Viñals^{1,2}

¹ *Supercomputer Computations Research Institute, Florida State University, Tallahassee, Florida 32306-4052,* ² *Department of Chemical Engineering, FAMU-FSU College of Engineering, Tallahassee, Florida 32310*

(June 26, 2018)

Abstract

We present a systematic nonlinear theory of pattern selection for parametric surface waves (Faraday waves), not restricted to fluids of low viscosity. A standing wave amplitude equation is derived from the Navier-Stokes equations that is of gradient form. The associated Lyapunov function is calculated for different regular patterns to determine the selected pattern near threshold. For fluids of large viscosity, the selected wave pattern consists of parallel stripes. At lower viscosity, patterns of square symmetry are obtained in the capillary regime (large frequencies). At lower frequencies (the mixed gravity-capillary regime), a sequence of six-fold (hexagonal), eight-fold, . . . patterns are predicted. The regions of stability of the various patterns are in quantitative agreement with recent experiments conducted in large aspect ratio systems.

Typeset using REVTeX

Parametrically driven surface waves (also known as Faraday waves) appear on the free surface of fluid layer which is periodically vibrated in the direction normal to the surface at rest. Above a certain critical value of the driving amplitude, the planar surface becomes unstable to a pattern of standing waves [1]. If the viscosity of the fluid is large, the bifurcating wave pattern consists of parallel stripes. At lower viscosity, patterns of square symmetry are observed in the capillary regime (large frequencies) [2]. At lower frequencies (the mixed gravity-capillary regime), hexagonal, eight-fold, and ten-fold patterns have been observed [3–5]. We present a weakly nonlinear analysis of the equations governing fluid motion that predicts stationary wave patterns with these symmetries. Their boundaries of stability agree quantitatively with experiments. [4,5]

Pattern selection in confined geometries can be often understood in terms of the spatial modes of the base state that become linearly unstable and the geometry of the system. Extended systems, on the other hand, allow a richer nonlinear competition of linearly unstable modes, in part due to the restoration of some of the symmetries of the original system that had been broken by the boundaries. The distinction can be further quantified by introducing the coherence length of the pattern ξ , the linear size of the system L , and the characteristic wavelength of the pattern $1/k_0$. Directional solidification from the melt is a typical example of a system in the limit $\xi_0 \ll 1/k_0 \ll L$, fact that follows from the extremely flat neutral stability curve [6]. Experiments often show a narrow distribution of wavelengths in the stationary state, the prediction of which has proven elusive. Attempts at deriving amplitude equations valid near onset have not been successful precisely because of the condition $\xi_0 \ll 1/k_0$. A typical and widely studied example of the intermediate range concerns Rayleigh-Bénard convection in large aspect ratio cells $1/k_0 \simeq \xi \ll L$. Although amplitude equations predict the existence of stable parallel rolls above onset, such a state is not generically observed in fluids of low or moderate Prandtl number except under carefully prepared initial conditions. Instead, a spatio-temporally chaotic state emerges that has been termed spiral defect chaos [7]. The role that long wavelength modes (or mean flow) play in the development of such a state is still a matter of research. Faraday waves, on the

other hand, are a prototypical case of a system with a large coherence length $\xi \gg 1/k_0$, and therefore one would expect that amplitude equations would allow quantitative predictions of pattern selection near onset. Furthermore, the physical system and the experimental conditions are completely determined by a few independent parameters that can be obtained with reasonable accuracy.

Progress in deriving suitable amplitude equations for Faraday waves has proved difficult. Since Faraday waves are almost a Hamiltonian system (weakly dissipative), most analyses are based on a hamiltonian description for the ideal (inviscid) limit, and treat viscous or dissipative effects as a perturbation [8,9]. The central question that arises in this case concerns the origin of any nonlinear saturation of the wave pattern. First, general symmetry considerations for Hamiltonian systems (“chiral symmetry”) prohibit cubic terms in standing wave amplitude equations [1,10]. In addition, it has been argued that linear viscous terms in the original equations governing Faraday waves only contribute linear damping terms to the amplitude equations [8]. These observations have contributed to the belief that saturation in near-Hamiltonian systems generically occurs through either nonlinear (cubic) viscous terms or fifth order hamiltonian terms, both of which are very difficult to obtain explicitly [8]. The issue, however, has remained somewhat controversial for the case of Faraday waves [9], and we mention, for example, two recent studies that considered non-dissipative cubic terms in the amplitude equation. Müller [11] has shown that the generic form of a cubic amplitude equation would allow patterns of standing waves with the observed symmetries, given suitable choices of the coefficients. A more recent analysis [12] explicitly addressed these issues in the limit of small fluid viscosity. A set of quasi-potential equations was derived by considering the rotational flow within a small viscous layer near the free surface, and assuming potential flow in the bulk. A standing wave amplitude equation was obtained with cubic order terms given explicitly.

Although this latter model predicted bifurcations to square and higher-symmetry patterns, it did rely on an uncontrolled approximation concerning nonlinear viscous terms. As a consequence, its region of validity is difficult to asses. In particular, it failed to yield the

observed stripe patterns at intermediate and large viscosities. We present here a general calculation that overcomes these difficulties, and that leads to the experimentally observed regular (periodic or quasi-periodic) standing wave patterns above onset. As part of the derivation, we also obtain an analytical expression for the linear threshold of instability, which was previously known only numerically [13]. Not being confined to small viscosities is also important for comparison with experiments since in this case it is easier to achieve the large aspect ratio limit, and hence to study pattern formation without the influence of side walls.

We consider an incompressible viscous fluid under vertical vibration $f \cos(\omega t)$ of amplitude f , and angular frequency ω . The fluid at rest has a free surface at $z = 0$, extends to $z = -\infty$, and is unbounded in the x - y direction. The equation governing fluid motion is

$$\partial_t \mathbf{u} + (\mathbf{u} \cdot \nabla) \mathbf{u} = -\frac{1}{\rho} \nabla p + \nu \nabla^2 \mathbf{u} + G(t) \hat{\mathbf{e}}_z,$$

with \mathbf{u} the velocity field, p the pressure, ρ and ν the density and kinematic viscosity of the fluid respectively, and $G(t) = -g - \frac{1}{2}f(e^{i\omega t} + e^{-i\omega t})$ the effective gravity. For f below the threshold of instability, the base state is $\mathbf{u} = 0$ and $p = \rho G(t)z$. We first eliminate the explicit dependence on the pressure by taking $-\nabla \times \nabla \times$ to obtain

$$\partial_t \nabla^2 \mathbf{u} - \nu \nabla^2 \nabla^2 \mathbf{u} = \nabla \times \nabla \times (\mathbf{u} \cdot \nabla) \mathbf{u}.$$

Here the continuity equation $\nabla \cdot \mathbf{u} = 0$ has also been used.

The position of the free surface is denoted by $\zeta(x, y)$, the unit normal $\hat{\mathbf{n}} = (-\partial_x \zeta, -\partial_y \zeta, 1)$, and the two tangential unit vectors are $\hat{\mathbf{t}}_1 = (1, 0, \partial_x \zeta)$ and $\hat{\mathbf{t}}_2 = (0, 1, \partial_y \zeta)$. Besides the null conditions at $z = -\infty$, there are three boundary conditions to be satisfied at the free surface,

$$\begin{aligned} \partial_t \zeta + (\mathbf{u} \cdot \nabla_H) \zeta &= w|_{z=\zeta} \\ \hat{\mathbf{t}}_m \cdot \mathbf{T} \cdot \hat{\mathbf{n}}|_{z=\zeta} &= 0, \quad m = 1, 2 \\ \hat{\mathbf{n}} \cdot \mathbf{T} \cdot \hat{\mathbf{n}}|_{z=\zeta} &= 2H\sigma, \end{aligned}$$

with $\nabla_H \equiv \hat{\mathbf{e}}_x \partial_x + \hat{\mathbf{e}}_y \partial_y$, \mathbf{T} the stress tensor with components $T_{ij} = [-p - \rho G(t)z] \delta_{ij} + \rho \nu (\partial_j u_i + \partial_i u_j)$, σ the surface tension, and $2H$ the mean curvature of the free surface [14].

First we consider the linear stability of a subharmonic standing wave,

$$w_0 = \cos(kx) \sum_{j=1,3,5,\dots} e^{ji\omega t/2} w_0^j(z) A_j + \text{c.c.},$$

where w_0 is the z -component of the velocity field, and a similar expansion for ζ_0 . Substitution into the linearized equation of motion, $(\partial_t \nabla^2 - \nu \nabla^2 \nabla^2) w_0 = 0$, and the linearized kinematic and tangential stress boundary conditions, $\partial_t \zeta_0 - w_0 = 0$ and $(\nabla_H^2 - \partial_z^2) w_0 = 0$, we find

$$w_0^j(z) = \nu(k^2 + q_j^2) e^{kz} - 2\nu k^2 e^{q_j z},$$

with $q_j^2 \equiv k^2 + ji\omega/2\nu$. Note that the boundary conditions at $z = \zeta$ have been expanded around $z = 0$. (Generalization to a finite fluid depth is straightforward: the term $d_1 e^{-kz} + d_2 e^{-q_j z}$ will also be in $w_0^j(z)$ with d_1 and d_2 to be determined by the additional boundary conditions at the bottom.)

The critical amplitude f_0 is determined by the linearized normal stress boundary condition, which is, after using the momentum equation to eliminate p_0 ,

$$\begin{aligned} & 2\rho\nu\nabla_H^2 \partial_z w_0 - \rho\partial_t \partial_z w_0 + \rho\nu\nabla^2 \partial_z w_0 + \rho g \nabla_H^2 \zeta_0 \\ & + \frac{1}{2}\rho f (e^{i\omega t} + e^{-i\omega t}) \nabla_H^2 \zeta_0 - \sigma \nabla_H^2 \nabla_H^2 \zeta_0 = 0. \end{aligned}$$

By substituting w_0 and ζ_0 into the above equation, we find for each harmonic $e^{ji\omega t/2}$,

$$\begin{aligned} H_1 A_1 - f A_1^* - f A_3 &= 0 \\ H_3 A_3 - f A_1 - f A_5 &= 0 \\ H_5 A_5 - f A_3 - f A_7 &= 0 \\ &\vdots \end{aligned} \tag{1}$$

with $H_j \equiv \left\{ \rho\nu^2 [4q_j k^4 - k(q_j^2 + k^2)^2] - \rho g k^2 - \sigma k^4 \right\} / \frac{1}{2}\rho k^2$. By truncating the set of equations (1) at some A_n , the system can be solved numerically as an eigenvalue problem. This is indeed what was done by Kumar and Tuckerman [13]. However we observe that after

truncation at A_n , $A_n = fA_{n-2}/H_n$, $A_{n-2} = fA_{n-4}/(H_{n-2} - \frac{f^2}{H_n})$, \dots . Therefore the set of equations can be rewritten as

$$\left(H_1 - \frac{f^2}{H_3 - \frac{f^2}{H_5 - \dots}} \right) A_1 - fA_1^* \equiv \bar{H}_1(k, f)A_1 - fA_1^* = 0,$$

so that for a given wavenumber k , the threshold of instability f_0 is given by

$$f_0 = |\bar{H}_1(k, f_0)|.$$

The complex amplitude A_j can be recursively obtained from Eq. (1) up to a real factor. For an infinite system the critical wavenumber k_{onset} is the wavenumber that corresponds to the lowest value of f_0 .

Consider first the limit of low viscosity, and define $\omega_0 \equiv \omega/2$ as the time scale, and k_0 from $\omega_0^2 = gk_0 + \sigma k_0^3/\rho$ as the length scale, and the dimensionless variables $\bar{k} = k/k_0$, $\gamma = 2\nu k_0^2/\omega_0$, $G = gk_0/\omega_0^2$, $\Sigma = \sigma k_0^3/\rho\omega_0^2$, and $\Delta = f_0 k_0/4\omega_0^2$. For a damping coefficient $\gamma \ll 1$ and k near k_{onset} , Δ_{onset} can be given explicitly as,

$$\Delta_{\text{onset}} = \gamma - \frac{1}{2}\gamma^{3/2} + \frac{11 - 2G}{8(3 - 2G)}\gamma^{5/2} + \dots,$$

with $0 \leq G \leq 1$ by definition. The dimensionless critical amplitude is proportional to $\gamma - \frac{1}{2}\gamma^{3/2}$ at small γ . While previous low damping calculations [8,12] only used the linear term to determine the location of the threshold, the first correction $-\frac{1}{2}\gamma^{3/2}$ can be a sizable contribution (e.g., a 15% difference at $\gamma = 0.1$). We also note that a similar calculation for the damped Mathieu equation leads to a threshold $\gamma + 3\gamma^2/64 + O(\gamma^3)$, in which the first correction term is of a different order and has a different sign.

To derive the amplitude equation we use the multiple scale approach [15]. The solvability condition in this case arises from the boundary conditions, not from the equation of motion as in most other cases. The velocity field is expanded as,

$$\mathbf{u} = \epsilon^{1/2}\mathbf{u}_0 + \epsilon\mathbf{u}_1 + \epsilon^{3/2}\mathbf{u}_2 + \dots,$$

with $\epsilon = (f - f_0)/f_0$, and similarly for p and ζ . Near threshold, i.e., for $\epsilon \ll 1$, we separate fast and slow time scales: $T = \epsilon t$; $\partial_t \rightarrow \partial_t + \epsilon\partial_T$. Spatial slow scales are not

included because only regular patterns are considered here. At order $\epsilon^{1/2}$ we recover the linear solution discussed above. Because we are interested in standing wave patterns with different symmetries, the solution at this order is written as a linear combination of waves with wavevectors \mathbf{k}_m of magnitude k_{onset} in different directions on the x - y plane,

$$w_0 = \sum_m \cos(\mathbf{k}_m \cdot \mathbf{r}) B_m(T) \sum_{j=1,3,5,\dots} e^{ji\omega t/2} w_0^j(z) e_j + \text{c.c.}$$

Here $B_m(T)$ are the *real* wave amplitudes, functions only of the slow time scale T , and e_j is A_j found in Eq. (1).

At order ϵ the equation of motion for w_1 becomes

$$\left(\partial_t \nabla^2 - \nu \nabla^2 \nabla^2 \right) w_1 = [\nabla \times \nabla \times (\mathbf{u}_0 \cdot \nabla) \mathbf{u}_0]_z. \quad (2)$$

The solution w_1 contains terms of the form $\cos((\mathbf{k}_m \pm \mathbf{k}_n) \cdot \mathbf{r})$ that incorporate couplings through stable modes, and that will contribute to the coefficients of the cubic terms later in the expansion. The particular solution w_{1p} is obtained by integrating Eq. (2), with the homogeneous solution w_{1h} chosen so that the boundary conditions are satisfied. Both the equation of motion and boundary conditions at this order become very complicated. In order to find w_1 in practice, we have developed a symbolic manipulation program specific to this case, and found the solution on a computer.

At order $\epsilon^{3/2}$ the equation of motion becomes

$$\begin{aligned} & \left(\partial_t \nabla^2 - \nu \nabla^2 \nabla^2 \right) w_2 \\ & = -\partial_T \nabla^2 w_0 + \{ \nabla \times \nabla \times [(\mathbf{u}_0 \cdot \nabla) \mathbf{u}_1 + (\mathbf{u}_1 \cdot \nabla) \mathbf{u}_0] \}_z. \end{aligned} \quad (3)$$

Only terms proportional to $\cos(\mathbf{k}_1 \cdot \mathbf{r})$ need to be considered in the solution for w_2 and ζ_2 ,

$$\begin{aligned} w_2 & = \cos(\mathbf{k}_1 \cdot \mathbf{r}) \sum_{j=1,3,5,\dots} e^{ji\omega t/2} \left[E_j + (a_j e^{kz} + b_j e^{q_j z}) C_j \right] \\ \zeta_2 & = \cos(\mathbf{k}_1 \cdot \mathbf{r}) \sum_{j=1,3,5,\dots} e^{ji\omega t/2} C_j. \end{aligned}$$

Here $E_j(z)$ comes from the direct integration of Eq. (3), and $a_j e^{kz} + b_j e^{q_j z}$ is the homogeneous solution that has the same form as the linear solution.

Using the kinematic and tangential stress boundary conditions at order $\epsilon^{3/2}$ we find (again with the symbolic manipulation program) a_j and b_j . The solution w_2 is finally inserted into the normal stress boundary condition at order $\epsilon^{3/2}$ to yield a system of equations for C_j which has the same left-hand side as Eq. (1) but with nonzero right hand side. Solving for C_j just like in Eq. (1), we obtain

$$\bar{H}_1 C_1 - f_0 C_1^* = F,$$

with F a function of the amplitude B_m . Since $f_0 = |\bar{H}_1|$, by requiring a nontrivial solution for C_1 we obtain the solvability condition $F\bar{H}_1^* + F^*f_0 = 0$, which yields a standing wave amplitude equation,

$$\frac{dB_1}{dT} = \alpha B_1 - g_0 B_1^3 - \sum_{m \neq 1} g(\theta_{m1}) B_m^2 B_1, \quad (4)$$

with θ_{m1} the angle between \mathbf{k}_m and \mathbf{k}_1 , and explicit expressions for the coefficients. Equation (4) is of gradient form, and can be derived from a Lyapunov function

$$\mathcal{F} = -\frac{1}{2}\alpha \sum_m B_m^2 + \frac{1}{4} \sum_m \sum_n g(\theta_{mn}) B_m^2 B_n^2, \quad (5)$$

which may be used to find the preferred pattern near threshold [1]. For regular patterns of N standing waves, \mathbf{k}_m form a regular polygon, and the B_m are constant.

We next turn to a comparison between the selected patterns predicted by Eq. (5), and two recent sets of systematic experimental surveys involving large aspect ratio systems, both of which aiming at addressing the issue of pattern selection over a wide range of experimental parameters [4,5]. Binks and van de Water [5] have focused on a low viscosity fluid [16], a large aspect ratio cell, and a layer depth much larger than the wavelength. When the driving frequency is decreased from 45Hz, a transition from a $N = 2$ square pattern to a $N = 3$ hexagonal pattern was observed at approximately 35Hz, and to a quasi-periodic $N = 4$ eight-fold pattern at approximately 29Hz [17]. Our prediction for these transitions based on Eq. (5) are 35.4 Hz and 28.7 Hz respectively. These results are also in good agreement with the earlier weak damping calculation [12] that predicted the same transitions at frequencies of 32.8 Hz and 27.9 Hz respectively.

A large aspect ratio experiment involving fluids of various viscosities has been carried out by Kudrolli and Gollub [4]. Although the fluid depth (0.3 cm) is smaller than the wavelength in the experiment (1–3 cm), the comparison is still illuminating. Figure 1 shows the symmetry of the preferred patterns predicted by our calculations in the parameter space defined by the viscosity of the fluid and the driving frequency (with $\rho = 0.95\text{g/cm}^3$ and $\sigma = 20.6\text{dyne/cm}$), and the experimentally observed patterns. Stripe patterns are preferred at high viscosity, whereas at low viscosity, hexagons (at low frequency) and squares (at high frequency) are observed. We also show the small region in which a sequence of quasiperiodic patterns are expected to be selected. The experimental results by Kudrolli and Gollub are shown as the symbols in the figure. We note an excellent agreement in the regions in which stripes, squares, and hexagons are observed, specially in view of the shallow fluid depth involved in the experiment. The shallowness of the layer probably accounts for the observation of a hexagonal pattern at $\nu = 1\text{cm}^2/\text{s}$ and low frequency, and not observing a quasiperiodic pattern for $\nu = 0.04\text{cm}^2/\text{s}$ and $f = 27\text{Hz}$. As noted above, the experiments by Binks and van de Water [5] did probe this latter region in a deep fluid layer, with their results agreeing with our predictions.

In summary, we have presented a nonlinear theory for Faraday waves in viscous fluids with no assumptions or approximations other than those inherent to the multiscale expansion. A set of standing wave amplitude equations has been obtained that is of gradient form. Minimization of the associated Lyapunov function leads to determination of the preferred pattern near threshold. The predicted patterns are in excellent agreement with recent experiments in large aspect ratio systems involving a range of fluid viscosities and driving frequencies.

This research has been supported by the U.S. Department of Energy, contract No. DE-FG05-95ER14566, and also in part by the Supercomputer Computations Research Institute, which is partially funded by the U.S. Department of Energy, contract No. DE-FC05-85ER25000.

REFERENCES

- [1] For a review see M.C. Cross and P.C. Hohenberg, *Rev. Mod. Phys.* **65**, 851 (1993).
- [2] See, e.g., N.B. Tuffillaro, R. Ramshankar, and J.P. Gollub, *Phys. Rev. Lett.* **62**, 422 (1989).
- [3] B. Christiansen, P. Alstrøm, and M.T. Levinsen, *Phys. Rev. Lett.* **68**, 2157 (1992).
W.S. Edwards and S. Fauve, *Phys. Rev. E.* **47**, R788 (1993), *J. Fluid Mech.* **278**, 123 (1994); M. Torres, G. Pastor, I. Jiménez, and F. Montero de Espinosa, *Chaos, Solitons & Fractals* **5**, 2089 (1995); T. Besson and W.S. Edwards, *Phys. Rev. E* **54**, 507 (1996).
- [4] A. Kudrolli and J.P. Gollub, *Physica D* **97**, 133 (1996).
- [5] D. Binks and W. van de Water, preprint (1996).
- [6] W.W. Mullins and R.F. Sekerka, *J. Appl. Phys.* **35**, 444 (1964).
- [7] S.W. Morris, E. Bodenschatz, D. Cannell, and G. Ahlers, *Phys. Rev. Lett.* **71** 2026 (1993); H.-W. Xi, J. Gunton, and J. Viñals, *Phys. Rev. Lett.* **71** 2030 (1993).
- [8] S.T. Milner, *J. Fluid Mech.* **225**, 81 (1991).
- [9] J.W. Miles, *J. Fluid Mech.* **248** 671 (1993); **269** 353 (1994).
- [10] P. Couillet, T. Frisch, and G. Sonnino, *Phys. Rev. E* **49**, 2087 (1994).
- [11] H.W. Müller, *Phys. Rev. E* **49** 1273 (1994).
- [12] W. Zhang and J. Viñals, *Phys. Rev. E* **53**, R4286 (1996); *J. Fluid Mech.* (in press).
- [13] K. Kumar and L.S. Tuckerman, *J. Fluid Mech.* **279**, 49 (1994).
- [14] H. Lamb, *Hydrodynamics*, 6th Ed., Dover (1945).
- [15] A.C. Newell and J.A. Whitehead, *J. Fluid Mech.* **38**, 279 (1969).
- [16] The fluid properties are: $\nu = 0.03397\text{cm}^2/\text{s}$ ($\gamma \sim 0.01 - 0.03$), $\rho = 0.8924\text{g}/\text{cm}^3$, and

$$\sigma = 18.3\text{dyne/cm.}$$

[17] In the experiment, patterns with $N = 5$ are observed around 27Hz. As it is also argued by the authors of the experiment, this could be attributed to finite size effects since \mathcal{F} for $N = 5$ is larger but very close to \mathcal{F} for $N = 4$. The difference at about 26 Hz is less than 0.2%.

FIGURES

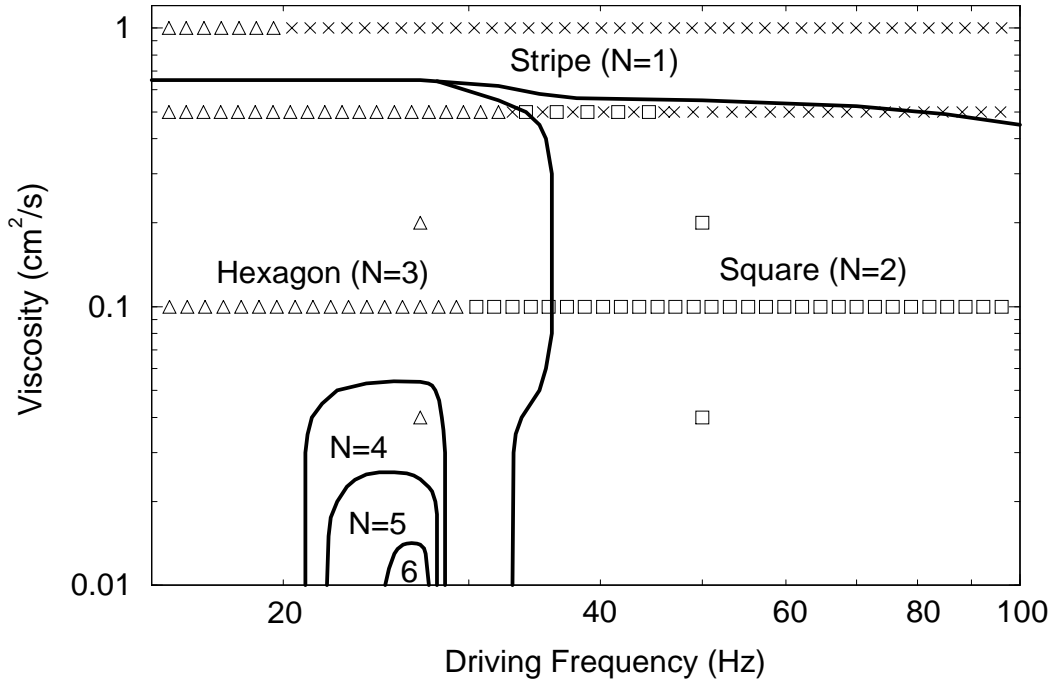


FIG. 1. Preferred patterns in viscosity-driving frequency space. Symbols represent the experimental results. \times =stripe, \square =square, and \triangle =hexagon. Alternating \times and \square indicate mixed-stripe-square states.